Modeling Dynamics of Colloidal Fouling of RO/NF Membranes with A Novel Collision-Attachment Approach

Junxia Liu [†], Zhihong Wang [†], Chuyang Y. Tang *[‡], James O. Leckie [§]

[†] Room 507, Block 2, School of Civil and Transportation Engineering, Guangdong University of Technology, No. 100 Waihuan Xi Road, Guangzhou Higher Education Mega Center, Guangzhou 510006, China

[‡] HW619B, Haking Wong Building, Department of Civil Engineering, The University of Hong Kong, Pokfulam Road, Hong Kong S.A.R., China

[§] Jerry Yang and Akiko Yamazaki Environmental and Energy Building, 473 Via Ortega, Room 261, Department of Civil and Environmental Engineering, Stanford University, Palo Alto, California 94305-4020, U.S.A.

*Corresponding Author:

Chuyang Y. Tang, tangc@hku.hk, +852 28591976

TABLE OF CONTENTS

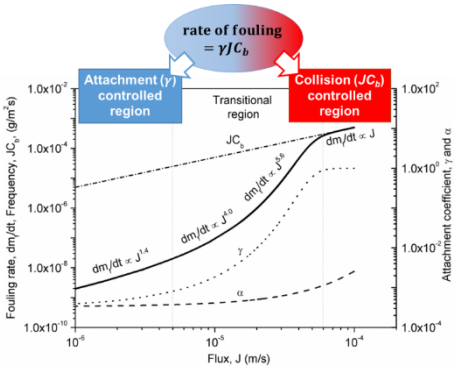

ABSTRACT

We report a novel collision-attachment approach for modeling the dynamics of colloidal fouling. The model treats fouling as a two-step process: colloidal particles colliding with a membrane surface followed by their attachment onto the surface. An attachment coefficient is adopted to describe the probability of successful foulant attachment for any given collision event, whose value can be determined by the classical Boltzmann distribution. Our model shows excellent agreement with experimental data in terms of both the kinetics of flux decline as well as foulant mass deposition. Modeling results reveal the critical roles of water flux and energy barrier in governing colloidal fouling. Greater water flux or lower energy barrier can lead to a collision-controlled condition, where severe fouling occurs and nearly all collision events lead to successful foulant attachment. On contrary, fouling is increasingly controlled by the probability of successful attachment at lower water flux and/or greater energy barrier. Our model provides deep insights into the various mechanisms governing the dynamics of colloidal fouling (i.e., concentration polarization, collision, and attachment) as well as the self-limiting fouling behavior under constant-pressure mode.

Introduction

Membrane fouling, which causes decreased productivity, increased energy consumption and shortened membrane lifetime, is a major obstacle for membrane separation.[1] Colloidal fouling is governed by a complex interplay of feed solution properties, membrane properties, and hydrodynamics conditions.[2] Ideally, the classical Navier-Stokes (NS) equation can model the fluid transport as well as fouling behavior during membrane filtrations:[3-5]

$$\rho\left(\frac{\partial \mathbf{u}}{\partial t}+(\mathbf{u}\cdot\nabla)\mathbf{u}\right)=-\nabla p+\mu\nabla^2\mathbf{u}+\mathbf{F} \qquad (1)$$

where the term $\mathbf{F}$ represents the interaction forces (i.e., surface interaction between particles and the membrane surface). A key challenge to implement NS-based fouling model is that the surface interaction forces typically act over nanometer scales[6-7], while the pressure force (∇p) and viscous force ($\mu\nabla^2\mathbf{u}$) act over much greater length scales.[8] Some simpler models, such as concentration polarization (CP)[9-11], mass transfer[12-14], and pressure drop[15-17], have also been proposed over the past years. However, such models often neglect the effect of the surface interactions and are thus unable to predict the effect of water chemistry on fouling.

A key milestone to comprehend colloidal fouling was the formulation of the critical flux theory by Field et al.[18] and Bacchin et al.[19]. According to these authors, there is no or minimal membrane fouling when the water flux is below a threshold value (i.e., the critical flux); the latter is strongly affected by the foulant-membrane interaction [20]. In a series of recent publications, Tang and coworkers[6, 20-23] proposed a simple limiting flux model considering the balance of hydrodynamic drag force and particle-membrane interaction force. This model helps to explain the existence of a maximum stable flux (i.e., the limiting flux) as well as the role of permeate flux and feed water chemistry in fouling. Nevertheless, Tang's model relies on a highly simplified assumption of constant interaction barrier force with

respect to the colloid-membrane distance, which is unlikely to be true in reality. In addition, the limiting flux theory can only predict the stable flux without being able to model the dynamic fouling process.

Much can be learnt from the classical coagulation theory, which models the conglomeration of colloidal particles via two key parameters, the particle-particle collision frequency and the attachment coefficient (α).[24-25] In this approach, α describes the probability of successful attachment for any given encounter of two particles (i.e., a collision event), and its value strongly depends on the interaction energy barrier and thus the water chemistry and properties of the particles. Since a membrane can be essentially viewed as an infinitely large particle, we are inspired to extend the classical collision-attachment approach to model the dynamics of membrane fouling.

In the current study, a novel model for the prediction of membrane fouling dynamics was developed based on the collision-attachment approach. A distinct feature of this study is that the interaction energy (instead of interaction forces in traditional fouling models) was used to predict the probability of particle attachment. Our modeling results provide deep insights into the roles of water flux and interaction energy on the progress of fouling as well as the self-limiting fouling behavior under constant-pressure mode.

Theory

Collision model. During membrane fouling, the rate of colloidal deposition onto a membrane surface (i.e., the rate of fouling, dm_f / dt) is given by:

$$\frac{dm_f}{dt} = \alpha J C_m \qquad (2)$$

where m_f is the mass of the deposited foulant, t is the filtration time, J is the permeate water flux, and C_m is the foulant concentration near the membrane surface. Here, the term JC_m is the mass flux of colloidal particles transported towards the membrane surface, which essentially characterizes the frequency of foulant-membrane collision events. At the same time, the attachment coefficient α is used to describe the probability of successful colloidal attachment for any given collision event; the value of α is therefore between 0 (collision never resulting in fouling) and 1 (collision always leading to colloidal attachment). In the following sections, we first use a CP model to relate C_m to the foulant concentration of the bulk feed solution C_b. We then develop a simple expression to show the dependence of α on the colloid-membrane interaction energy.

Bulk solution CP model. We perform a mass balance to determine the membrane surface concentration C_m (Supporting Information S1):

$$D\frac{dC}{dx} = JC - JC_P - \alpha JC_m \qquad (3a)$$

where D is the diffusion coefficient of the foulant particles, C is the foulant concentration at a distance of x away from the membrane surface, and C_p is the foulant concentration in the permeate water. The foulant concentration at $x = 0$ is defined as the membrane surface concentration C_m, i.e.,

$$C(x = 0) = C_m \qquad (3b)$$

In addition, the boundary condition for Eq. 3a is given by:

$$\text{and} \quad C(x = \delta) = C_b \qquad (3c)$$

Eq. 3 is essentially similar to conventional CP models[8, 26-28], where the convection of foulants towards a membrane (JC) is balanced by the diffusion of foulants away from the membrane

($D \cdot dC/dx$) and the additional sink terms (e.g., the loss of foulants to the permeate water, JC_p). In the current study, we also include the loss of foulants from the solution phase due to their deposition on the membrane, which is given by αJC_m according to Eq. 1.

By integrating Eq. 3a and substituting the boundary conditions Eq. 3b,c, one can obtain:

$$\frac{C_m - C_p - \alpha C_m}{C_b - C_p - \alpha C_m} = \exp\left(\frac{J}{k}\right) \quad (4)$$

The term J/k in Eq. 4 is also known as the Péclet number (*Pe*), which is the ratio of convective transport to diffusive transport in the boundary layer. The mass transfer coefficient *k* is related to the hydrodynamic boundary thickness δ by: [8, 29]

$$k = \frac{D}{\delta} \quad (5)$$

The diffusion coefficient *D* in Eq. 5 can be calculated according to the Stokes-Einstein relationship:[26]

$$D = \frac{k_B T}{3\pi\mu d_p} \quad (6)$$

where k_B and *T* are the Boltzmann's constant and absolute temperature, respectively; μ and d_p are the solution viscosity and colloidal particle diameter, respectively.

Eq. 4 takes a similar form compared to the conventional CP models (e.g., film theory $C_m/C_b = \exp(J/k)$ or $(C_m - C_p)/(C_b - C_p) = \exp(J/k)$) [8, 26-28], with the exception that a term αC_m is included to account for the additional depolarization mechanism due to foulant deposition. In RO and NF processes, the foulant concentration C_p in the permeate is negligible compared to C_b and C_m. Thus, Eq. 4 can be further simplified to:

$$C_m = \frac{C_b \exp\left(\frac{J}{k}\right)}{1-\alpha+\alpha\exp\left(\frac{J}{k}\right)} \quad (7)$$

Attachment model. To determine the attachment coefficient α, we adopt the classical Boltzmann distribution that describes the frequency distribution of particles in a system over various possible states.[30] The Boltzmann equation has also been used to describe the number density of particles in different energy states during particle-particle attachment in coagulation.[25] In the context of colloidal fouling, colloids can exist in two states: colloidal particles attached to a membrane surface (N_1) and free colloidal particles in the solution (N_2). For a free colloidal particle to attach onto the membrane, it has to overcome the potential energy barrier ΔE_b arising from the colloid-membrane interaction. In addition, the hydrodynamic drag force acting on the colloidal particle provides an additional potential energy ΔE_d that promotes its attachment. Thus, colloidal particles will distribute among the free and attached states in a statistical manner in accordance to the Boltzmann equation as follows:

$$\frac{N_1}{N_2} = \exp\left(-\frac{\Delta E_b - \Delta E_d}{k_B T}\right) \quad (8)$$

where N_1 denotes the number of attached colloids and N_2 denotes the number of free colloids. Accordingly, the attachment coefficient α is given by:

$$\alpha = \frac{N_1}{N_1 + N_2} \quad (9)$$

It is worthwhile to note that the Boltzmann equation captures the effect of Brownian motion of the foulants in a statistical manner. Indeed, the classical Stokes-Einstein relationship (Eq. 6)

states that the diffusion coefficient of a colloidal particle is directional proportional to the k_BT energy.

ΔE_d in Eq. 8 arises from the hydrodynamic drag force ($3\pi\mu d_p J$) acting on colloidal particle:

$$\Delta E_d = 3\pi\mu d_p J \times l_d = \beta J \tag{10}$$

where μ is the viscosity of the solution, l_d is the relative displacement of the colloidal particle under the influence of the drag force, and β is a proportionality coefficient ($\beta = 3\pi\mu d_p l_d$). Combining Eqs. 8 - 10 leads to a simple equation relating the attachment coefficient α to two dimensionless numbers, i.e., the energy barrier number ($\Delta E_b / k_B T$) and the drag number ($\beta J / k_B T$), as follows:

$$\alpha = \frac{1}{1 + \exp\left(\frac{\Delta E_b}{k_B T} - \frac{\beta J}{k_B T}\right)} \tag{11}$$

Substituting Eq. 7 and Eq. 11 into Eq. 2, we further obtain

$$\frac{dm_f}{dt} = \gamma J C_b \tag{12a}$$

$$\gamma = \frac{1}{1 + \exp\left(\frac{\Delta E_b}{k_B T} - \frac{\beta J}{k_B T} - \frac{J}{k}\right)} \tag{12b}$$

In the above derivation, two key assumptions are involved. Firstly, we assume a dilute foulant solution. This assumption implies a relatively large average distance between foulant particles such that the effect of foulant-membrane interaction dominates over that of foulant-foulant interaction in the solution.[2] The aggregation of foulants in the boundary layer is not considered in the current study.[2, 31] We further assume that the effect of inertial lift and shear-induced diffusion can be neglected. This assumption is reasonable for colloids of small size

(<< 100 nm).[2] Where large colloids of ~ or > 100 nm are considered, Eq. 10 needs to be modified to incorporate the additional effects of inertial lift and shear-induced diffusion.[32-34]

According to Eq. 12a, the rate of fouling (dm_f / dt) is proportional to the apparent amount of foulant introduced to the membrane surface (i.e., the apparent collision frequency JC_b) as well as the apparent attachment coefficient after accounting for the effect of CP (γ). The latter further depends on the energy barrier number, the drag number, and the Péclet number (Eq. 12b). The energy barrier number $\Delta E_b / k_B T$ scales the interaction potential energy barrier to the thermal vibration energy. The value of ΔE_b is strongly dependent on the properties of the particle and membrane as well as the solution chemistry, and it can be either calculated by classical DLVO (or XDLVO) theory[35-37] or measured experimentally[38-41]. A larger ΔE_b indicates a more repulsive interaction between a colloidal particle and the membrane surface, which helps to prevent its attachment onto the surface. On contrary, a lower ΔE_b tends to promote fouling by increasing the success rate of attachment. The drag number $\beta J / k_B T$ accounts for the effect of hydrodynamic drag in overcoming the potential energy barrier, and the Péclet number accounts for the effect of CP. A greater water flux leads to a more severe fouling by simultaneously increasing the collision frequency (Eq. 2), the attachment coefficient (Eq. 11), and the CP (Eq. 4).

Eq. 12a,b provides a useful means to model the dynamic process of membrane fouling. Consider a constant pressure condition, the water flux at any time *t* is given by:

$$J = \frac{\Delta P}{\mu\left(R_m + R_f\right)} \tag{13}$$

where ΔP is the applied pressure and R_m is the hydraulic resistance of the virgin membrane. The hydraulic resistance R_f of the foulant layer is related to the amount of foulant mass deposition m_f by the specific cake resistance α_f :[42]

$$R_f = \alpha_f m_f \quad (14)$$

Eq. 12-14 can be solved iteratively, e.g., using a spreadsheet to obtain water flux and foulant mass deposition as a function of time.

Experimental Validation

To validate the collision-attachment fouling model, we compared our model prediction with the experimental data published in a prior study.[20] Specifically, a commercial nanofiltration membrane NF90 was fouled by purified Aldrich humic acid (PAHA) with/without the addition of Ca^{2+} under applied pressures ranging from 50 to 300 psi (i.e., 345-2070 kPa). The PAHA was extensively pretreated in accordance to Tang et al.[43] to remove impurities such as metals and ash contents. The resulting PAHA was negatively charged, with a charge density of 4.01 meq/g in a 10 mM NaCl solution at pH 7.[6] The charge density was reduced to -2.51 meq/g when a 1 mM Ca^{2+} was present in the solution, which is attributed to the binding of calcium to PAHA macromolecules to partially neutralize their charge.[6] Similarly, the negative surface charge of NF90 was also significantly neutralized in the presence of 1 mM Ca^{2+}.[42] Other properties of the foulant and the membrane can be found in our series of characterization papers.[6, 20, 42-45]

The detailed parameters and procedures for modeling the fouling dynamics are presented in Supporting Information S2 and S3, respectively. Our model was able to well predict both the fouling dynamics (Figure 1a,b) and foulant deposition on membrane surface (Figure 1c). In general, flux was more stable at lower applied pressure (lower initial flux), which agrees well

with existing critical flux[18] and limiting flux[20] theories. The addition of 1 mM Ca^{2+} in the feed solution led to more severe flux reduction, which is accompanied with greater foulant mass deposition. According to our prior studies, Ca^{2+} form complexes with PAHA and the NF membrane and partially neutralizes their negative charge, leading to reduced electrostatic repulsion between PAHA and the membrane surface.[6, 43] Such effect of water chemistry is reflected by the reduced value of ΔE_b (from 7.9 k_BT to 4.9 k_BT, see Supporting Information S2) in the current study. Our model is capable of predicting not only the dynamics of fouling but also the effect of water chemistry.

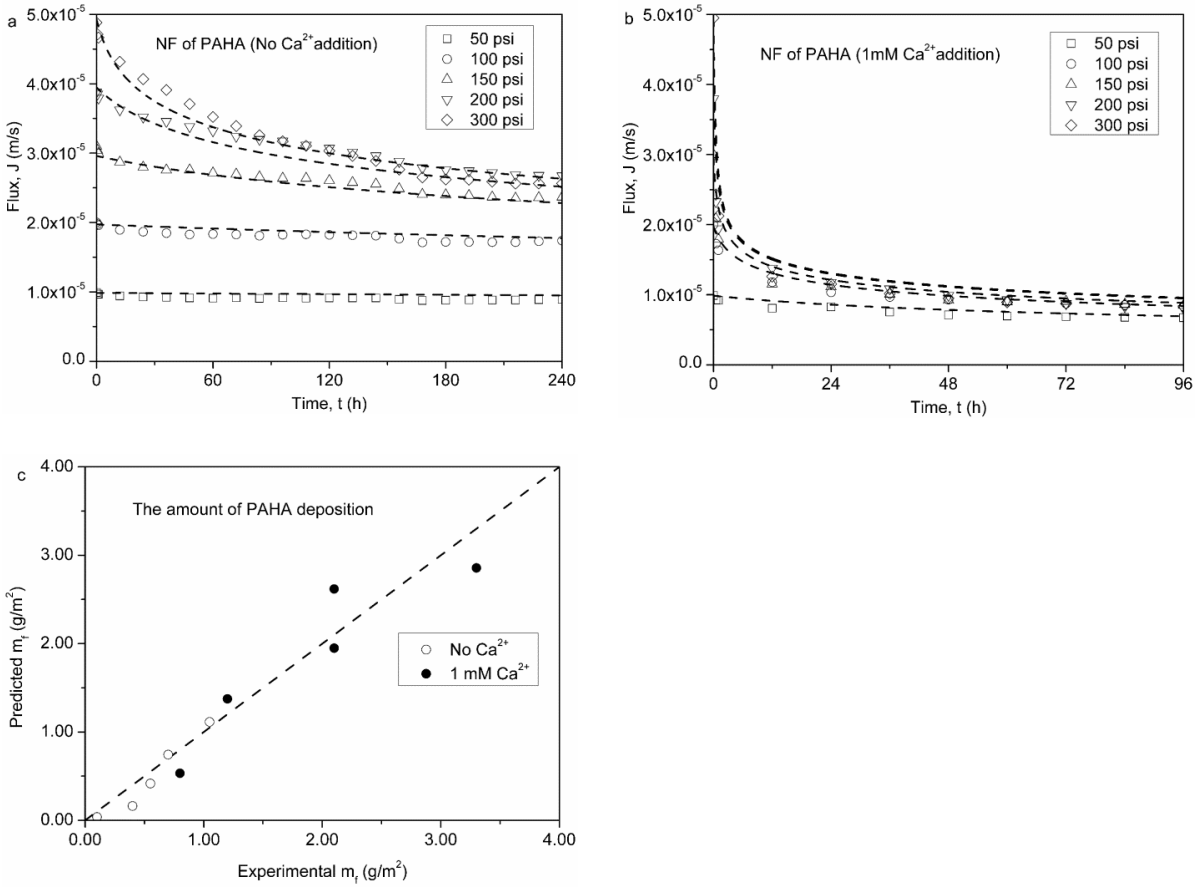

Figure 1. Model validation for a nanofiltration membrane fouled by purified Aldrich humic acid (PAHA). Permeate flux versus time (a) without Ca^{2+} addition or (b) with the addition of 1 mM Ca^{2+}; (c) PAHA foulant mass deposition. The experimental data (scattered dots) are obtained from reference.[20] Detailed simulation conditions are shown in Table S1 of the Supporting Information.

Simulation Results and Discussion

Role of permeate flux on fouling. We applied the collision-attachment fouling model to simulate the dynamic fouling process by colloidal particles (Table 1). Figure 2 shows the effect of initial flux (J_0 =10 - 70 μm/s) on the flux behavior of the membrane. With a low J_0 of 10 μm/s, permeate water flux remains stable over the entire 100-h fouling duration. Flux becomes increasingly unstable for greater J_0 values. Whereas flux decline is relatively mild at J_0 = 30 μm/s, rapid flux declines occur at J_0 = 50 and 70 μm/s. The rate of fouling reduces as fouling proceeds, which is attributed to the reduced flux. At longer duration, flux becomes relatively stable, revealing the "self-limiting" nature of fouling under constant pressure conditions.[6] Despite of their distinctively different initial flux values, the flux curves converge to a nearly identical stable flux at 100 h for $J_0 \geq 30$ μm/s. Such flux behavior essentially conforms to the limiting flux theory: (1) permeate flux remains stable if J_0 is lower than the limiting flux J_L; (2) permeate flux approaches asymptotically to the limiting flux if $J_0 > J_L$. The limiting flux behavior during colloidal fouling had been experimentally observed by Tang and co-workers and had been explained on the basis of a simple force balance between the hydrodynamic drag force that promotes fouling and the barrier force that resists fouling. [6, 20-23] In the current study, we demonstrate the limiting flux behavior on the basis on collision-attachment model. According to this model, lower flux results in less fouling due to three simultaneous effects: (1) reduced apparent collision rate JC_b (Eq. 12a); (2) reduced concentration polarization C_m/C_b (Eq. 4 and Eq. 12b); and (3) reduced attachment coefficient α (Eq. 11).

Table 1 Parameters for model simulation

	Parameters [a]	Value	Remarks
Solution properties	T	298.15 K (25 °C)	Ref. [20]
	μ	8.9×10^{-4} Pa.s	Ref. [20]
	C_b	5.0 g/m^3 (5 mg/L)	Ref. [20]
Operation Conditions	u	0.2 m/s (20 cm/s)	Ref. [20]
	$\triangle P$	40-4000 kPa	See Note [b]
	R_m	4.50×10^{13} m^{-1}	Ref. [20]
	α_f	3.0×10^{13} m/g	Ref. [42] and Note [c]
Spacer Filaments	h_{sp}	1.15×10^{-3} m	Ref. [29]
	d_{sp}	6.00×10^{-4} m	Ref. [29]
	a_{sp}	2.95×10^{-3} m	Ref. [29]
	θ	90°	Ref. [29]
Mass transfer	d_p	2.0×10^{-8} m	
	D	2.45×10^{-11} m^2/s	Ref. [26]
	k	6.70×10^{-6} m/s	Ref. [29]
Energy	k_BT	4.11×10^{-21} J	
	β	$4.19\times10^{-9}\times d_p$	Table S1
	$\triangle E_b$	0-16 k_BT	See Note [d]

Notes:

a. Absolute temperature (T), Solution viscosity (μ), Bulk foulant concentration (C_b), Crossflow velocity (u), initial flux(J_0), Membrane intrinsic resistance (R_m), Specific cake resistance (α_f), Spacer thickness (h_{sp}), Filament diameter (d_{sp}), Mesh size (a_{sp}), Filaments intersection angle (θ), Particle size (d_p), Diffusion coefficient(D), Mass transfer coefficient (k), Boltzmann's constant (k_B), Drag energy coefficient (β), Energy barrier ($\triangle E_b$).

b. This pressure range corresponds to permeate water flux ranging from 1×10^{-6} to 1×10^{-4} m/s (i.e., 3.6 – 360 L/m^2.h), which covers the typical water flux used in RO and NF operations.

c. For simplicity, we assume a constant α_f for the model simulation. Please also refer to the Implication section for further discussion of treating α_f as a function of ΔP.

d. The range of $\triangle E_b$ is chosen according to the fitted value for PAHA (Table S1) and previous reports on the energy barrier for protein[46], polysaccharide [47] as well as soluble microbial products [48] in membrane fouling.

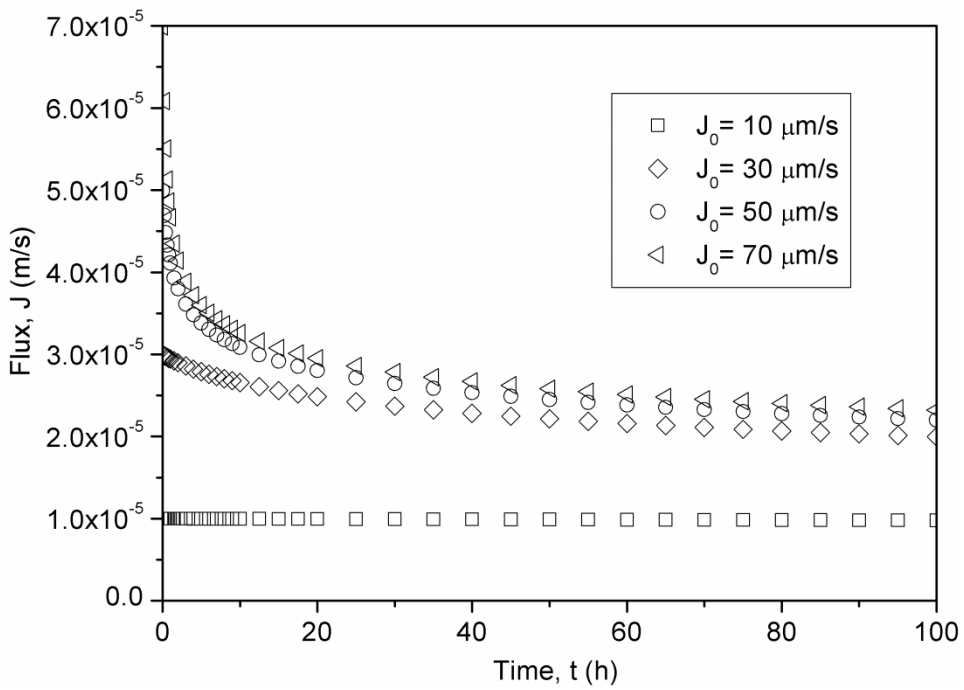

Figure 2. Effect of initial water flux on colloidal fouling. Simulation conditions: $\triangle E_b = 8k_BT$; see other parameters in Table 1.

To further resolve the role of permeate water flux on fouling, we plot the rate of fouling dm_f/dt and the apparent collision frequency JC_b as a function of water flux J on a log-scale in Figure 3. In the same figure, we also show the actual and apparent attachment coefficients α and γ, respectively, where the difference between α (Eq. 11) and γ (Eq. 12b) is attributed to concentration polarization. Overall, the rate of fouling increases with greater water flux, reflecting the compounded effects of increased collision frequency, more severe concentration polarization, and increased attachment coefficient. However, Figure 3 can be divided into three distinct regions:

- Region I (collision controlled region) at large J. This region is characterized by $\gamma \approx 1$ and large values of dm_f/dt. Region I represents a highly unstable flux condition, with almost every single collision event leading to a successful foulant attachment and thus nearly all the foulants in the cross flow system depositing onto the membrane surface.

Consequently, the rate of fouling is given by $dm_f/dt = JC_b$ in this region, revealing that the rate of fouling is ultimately controlled by the frequency of collision in this region.

- Region II (attachment controlled region) at low J. In contrast to Region I with $\gamma \approx 1$, Region II is characterized by small γ values (~ or < 10^{-3}). In addition, the minor difference between α and γ reveals relatively mild concentration polarization. In this region, the rate of fouling is proportional to $J^{1.4}$. Since the rate of foulant deposition is governed by γJC_b, the additional power number of 0.4 is attributed to the dependence of γ on J.
- Region III (transitional region) at intermediate J. A transitional region exists between the high flux region (collision controlled) and the low flux region (attachment controlled). In this region, the apparent attachment coefficient γ increases dramatically with the increase of J. Meanwhile, the difference between α and γ becomes progressively larger at high J, reflecting the presence of severe concentration polarization.

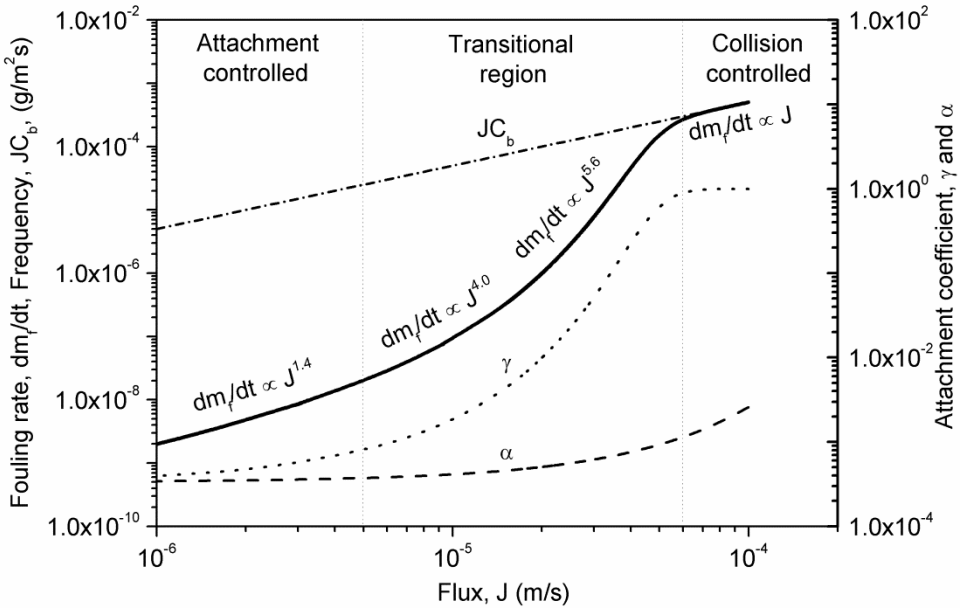

Figure 3. Effect of permeate water flux on the rate of fouling dm_f/dt, the apparent collision frequency JC_b, the actual attachment coefficient α, and the apparent attachment coefficient γ. Simulation conditions: $\triangle E_b = 8k_BT$; see other parameters in Table 1.

Role of energy barrier on fouling. Figure 4 reveals the critical role of energy barrier in membrane fouling. A greater energy barrier leads to less fouling and more stabilized membrane flux, which can be explained by the more repulsive interaction between the foulant and the membrane surface. Even though the apparent frequency of collision is not affected by energy barrier, Figure 5a shows that a larger $\triangle E_b$ value results in dramatic reduction in the attachment coefficients α (Eq. 11) and γ (Eq. 12b). Increasing $\triangle E_b$ from 0 to 16 k_BT corresponds to a reduction in the actual attachment coefficient α by more than 6 orders of magnitude. The effect of energy barrier on the apparent attachment coefficient γ is somewhat milder (particularly at higher permeate flux), which can be attributed to the important role of concentration polarization. Despite the very low α value at high energy barriers (e.g., 16 k_BT), concentration polarization of foulants causes a much higher foulant concentration near the membrane surface than the bulk concentration, leading to a significantly larger γ value and thus accelerated foulant deposition.

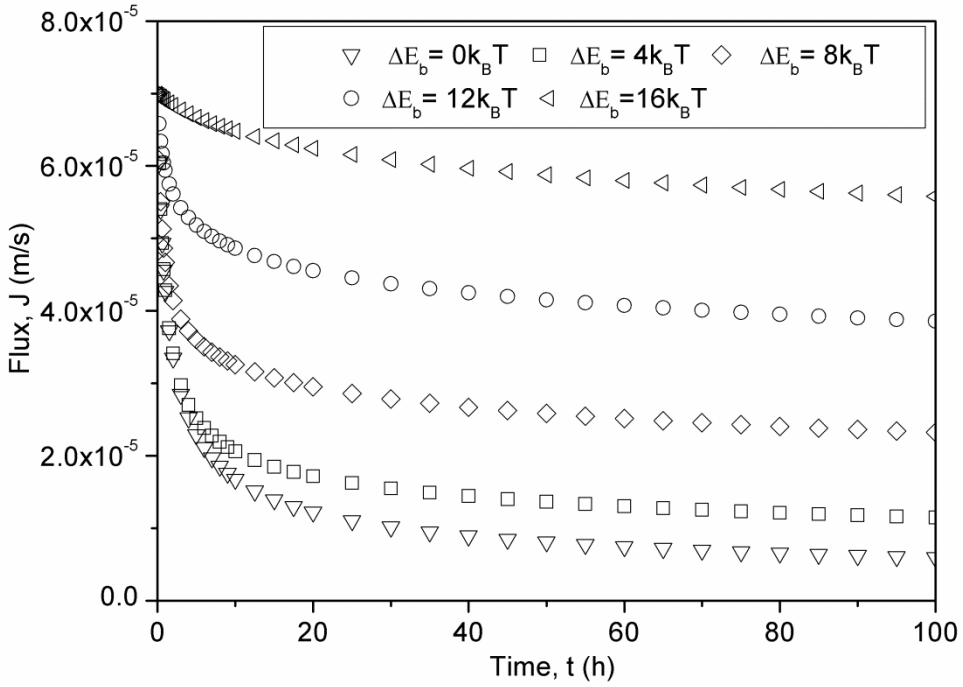

Figure 4. Effect of energy barrier on colloidal fouling. Simulation conditions: initial flux = 70 μm/s; see other parameters in Table 1.

The shape of the rate of fouling curves (Figure 5b) closely resembles that of the γ curves (Figure 5a). At $\triangle E_b = 0$ (lack of repulsive foulant-membrane interaction), the dm_f/dt curve nearly overlap with the JC_b line. Since the latter represents the frequency of apparent collision, this result suggests that almost all the foulants transported towards the membrane surface lead to successful foulant deposition, which is a highly unfavorable condition defined as "collision-controlled" in current study. Increasing energy barrier or lowering water flux dramatically reduces the rate of fouling by lowering the apparent attachment coefficient, resulting in increasingly "attachment-controlled" conditions. Such classification of fouling into "collision-controlled" and "attachment-controlled" is somewhat analogous to the conventional classification of "diffusion-controlled" and "reaction-controlled" reactions. [49] The terms "diffusion-controlled" and "reaction-controlled" have also been well accepted in the field of coagulation, which are used to describe the mechanism that limits particle-particle conglomeration (i.e., rate of transport vs. rate of attachment). [50] In the current study, Figure 5b clearly depicts the interplay of energy barrier (resisting membrane fouling) and permeate flux (promoting membrane fouling) on determining the rate of fouling. It is also interesting to note the similar power law relationship of $dm_f/dt \propto J^{1.4}$ for the "attachment-controlled" regions for $\triangle E_b$ ranging from 4 k_BT to 12 k_BT. While the exact reason for the power coefficient of 1.4 is unknown, the additional 0.4 can be attributed to the dependence of γ on J. As shown in Figure 5a, the γ curves (except the one for $\triangle E_b = 0$) have similar slope at low permeate flux (approximately 0.4). The generality of this power dependence needs to be further confirmed by additional experimental studies.

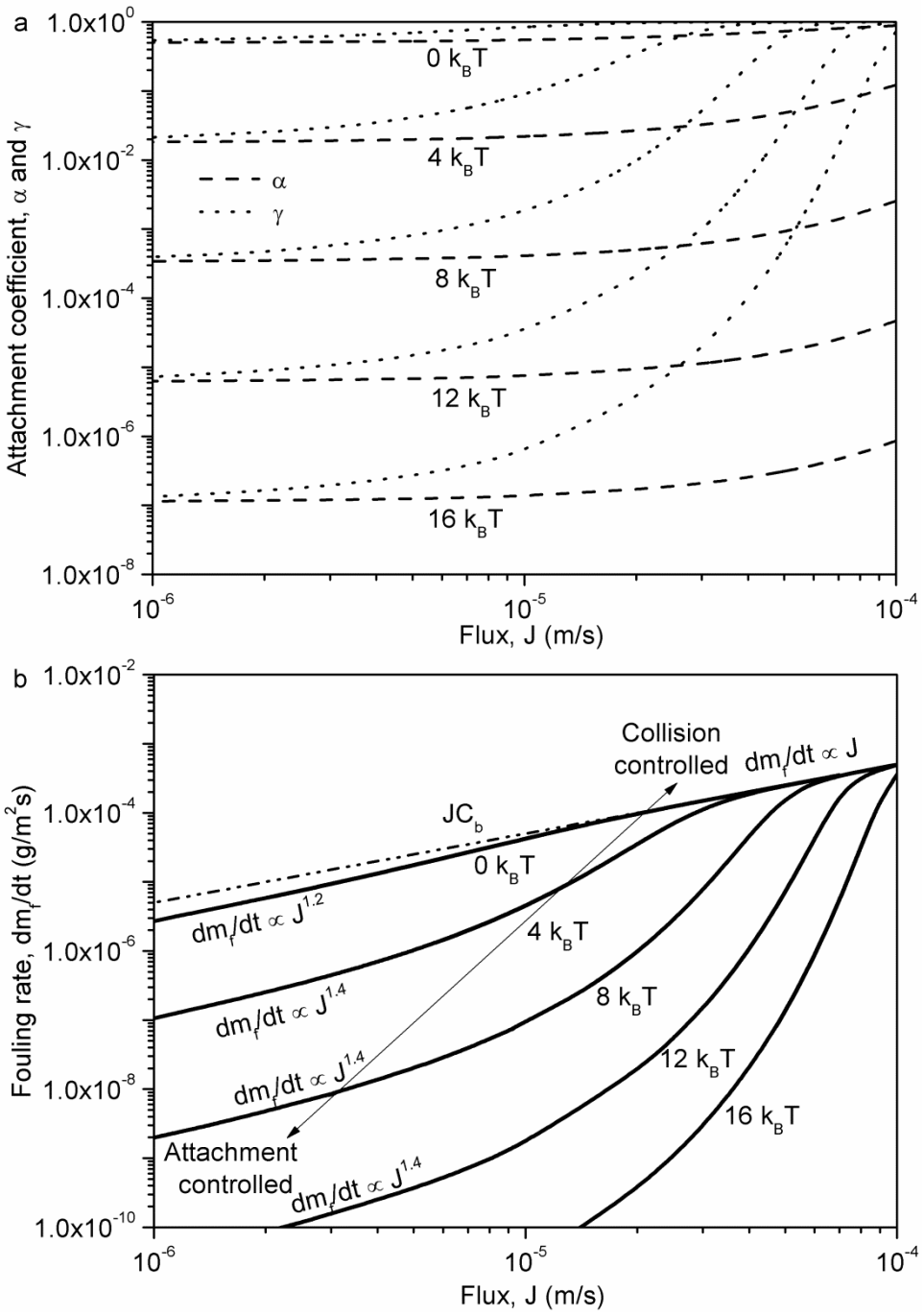

Figure 5. Effect of energy barrier on the attachment coefficients α and γ (a) and the rate of fouling dm_f/dt (b). See simulation parameters in Table 1.

Limiting flux and its dependence on energy barrier. In Figure 5b, the rate of fouling becomes increasingly slower when the permeate water flux is reduced, which can lead to a self-limiting flux behavior as reported in the literature.[6] The limiting flux can be operationally defined as the flux corresponding to a sufficiently slow rate of foulant deposition. As an

example, Figure 6 shows the limiting flux as a function of energy barrier using a threshold dm_f/dt value of 5×10^{-7} g/m^{2}s. The limiting flux is nearly 0 at $\Delta E_b = 0$, indicating a highly unstable flux condition with the lack of repulsive surface interaction. The value of limiting flux increases at high energy barrier, which agrees well with the experimental observations reported in the literature.[6] It is interesting to note that the limiting flux value is linearly dependent on the energy barrier for $\Delta E_b > 6k_BT$. The large energy barrier allows a relatively high stable permeate water flux and thus high frequency of collision. Consequently, the only way to reach the low threshold dm_f/dt value is to ensure a sufficiently small value of γ, which requires a large exponent ($\Delta E_b / k_BT - \beta J / k_BT - J / k$) in Eq. 12b and thus a linear dependence of limiting flux on energy barrier. In contrast, at low energy barrier, both JC_b and γ are small, leading to a non-linear relationship between limiting flux and energy barrier.

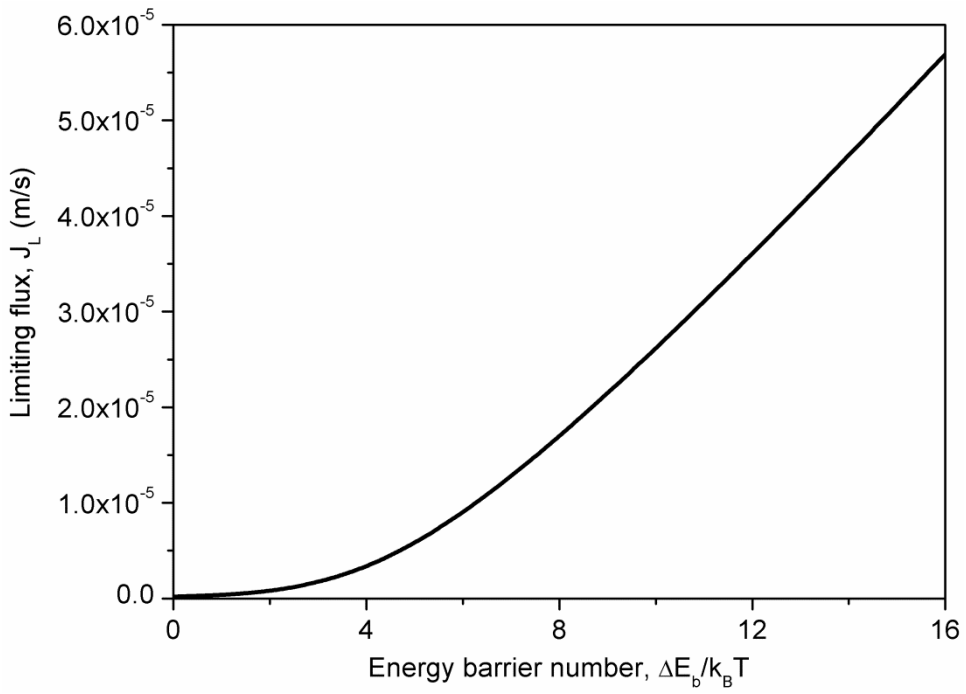

Figure 6. Dependence of limiting flux on energy barrier. See simulation parameters in Table 1. A threshold fouling rate of 5.0×10^{-7} g/m^{2}s is applied.

Implications

A novel collision-attachment model is developed in the current study, in which the probability of colloidal deposition is determined by a Boltzmann distribution based on the interplay of energy barrier and hydrodynamic drag. Earlier studies have demonstrated that $\triangle E_b$ can be related to the feed solution chemistry (e.g., using DLVO/XDLVO[35-37] or AFM interaction force measurements[38-41]). Thus, the inclusion of energy barrier in the collision-attachment model provides a convenient way to model the effect of water chemistry on the dynamics of fouling (see the example in Experimental Validation) as well as the limiting flux behavior. Tang et al. [6] demonstrated experimentally that increasing pH and reducing calcium concentration help to enhance the repulsive interaction between humic acid and membrane and thus improve the membrane flux stability. The collision-attachment model developed in the current study coupled with DLVO/XDLVO theory provides a potential way to quantitatively model the effect of water chemistry on the fouling dynamics.

Although the current study focused primarily on colloidal fouling under constant pressure conditions, the collision-attachment model can also be applied to simulate the change of applied pressure over time under constant flux conditions (see the procedures in Supporting Information S3). For incompressible foulant cake layer (i.e., α_f does not change with respect to $\triangle P$), Fig. 7 shows the applied pressure increases linearly over time under a constant flux operation. Indeed, both the frequency of collision and the attachment coefficient are constant at the fixed water flux. Compressible foulant cake layers can also be simulated by assuming $\alpha_f = \alpha_0 (\triangle P/\triangle P_0)^s$, where s indicates the degree of cake compressibility.[2, 51] In Fig. 7, the compressible cake layers (s = 0.5 and 1) show more rapid increase in $\triangle P$ at longer fouling duration. Such self-accelerating fouling behavior under the constant flux mode is in direct contrast to the self-limiting behavior (Fig. 2) under the constant pressure mode. Our results

401 also reveal the more critical need for flux management (e.g., operating below the limiting
402 flux) under the constant flux mode to avoid the undesirable self-accelerating behavior.
403

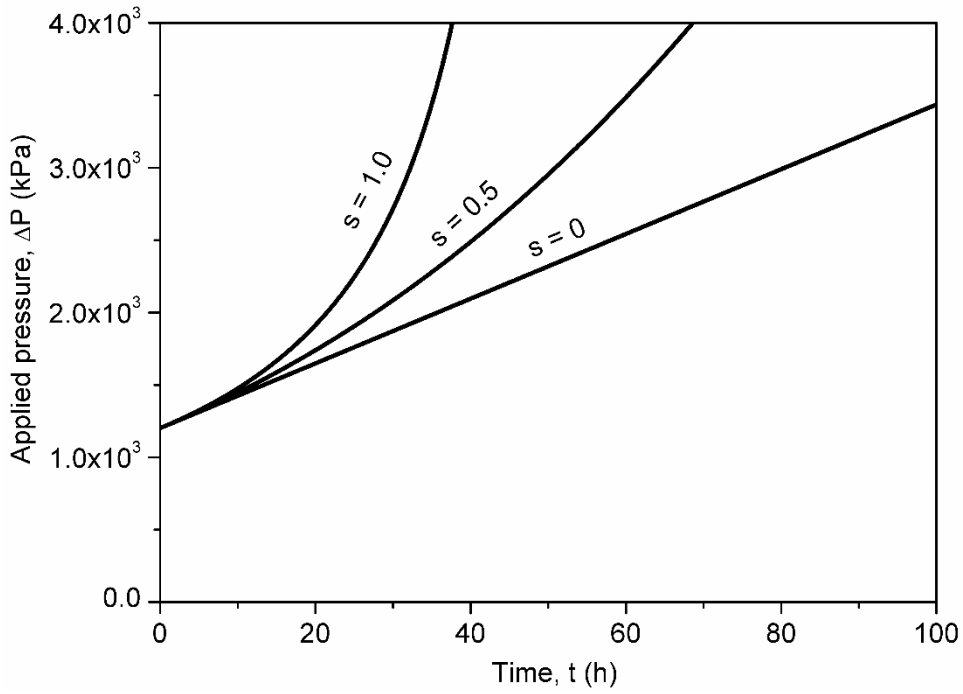

404

405 Figure 7. Simulating the effect of cake compressibility under constant flux operation.
406 Simulation conditions: J = 30 μm/s, $\triangle E_b = 8k_BT$; see other parameters in Table 1.
407

408 ## Acknowledgements

409 This research was financially supported by the Strategic Interdisciplinary Research Scheme
410 of the University of Hong Kong (No. 102009619) and National Natural Science Foundation
411 of China (No. 51708130). The authors also thank Dr. Qianhong She for his assistance in mass
412 transfer calculations in spacer filled channels.

413

414 ## Supporting Information

S1. Concentration polarization; S2. Parameters for model validation; S3. Modeling fouling dynamics; S4. Fitting experimental data with the Hermia model. This material is available free of charge via the Internet at http://pubs.acs.org.

References

1. Krzeminski, P.; Leverette, L.; Malamis, S.; Katsou, E., Membrane bioreactors - A review on recent developments in energy reduction, fouling control, novel configurations, LCA and market prospects. *J. Membr. Sci.* **2017,** *527*, 207-227.
2. Tang, C. Y.; Chong, T.; Fane, A. G., Colloidal interactions and fouling of NF and RO membranes: a review. *Adv. Colloid Interface Sci.* **2011,** *164* (1), 126-143.
3. Ghidossi, R.; Veyret, D.; Moulin, P., Computational fluid dynamics applied to membranes: State of the art and opportunities. *Chem. Eng. Process.* **2006,** *45* (6), 437-454.
4. Belfort, G.; Davis, R. H.; Zydney, A. L., The behavior of suspensions and macromolecular solutions in crossflow microfiltration. *J. Membr. Sci.* **1994,** *96* (1-2), 1-58.
5. Belfort, G., Fluid mechanics in membrane filtration: recent developments. *J. Membr. Sci.* **1989,** *40* (2), 123-147.
6. Tang, C. Y.; Kwon, Y.-N.; Leckie, J. O., The role of foulant–foulant electrostatic interaction on limiting flux for RO and NF membranes during humic acid fouling—theoretical basis, experimental evidence, and AFM interaction force measurement. *J. Membr. Sci.* **2009,** *326* (2), 526-532.
7. Brant, J. A.; Childress, A. E., Assessing short-range membrane–colloid interactions using surface energetics. *J. Membr. Sci.* **2002,** *203* (1), 257-273.
8. Hoek, E. M. V.; Kim, A. S.; Elimelech, M., Influence of crossflow membrane filter geometry and shear rate on colloidal fouling in reverse osmosis and nanofiltration separations. *Environmental Engineering Science* **2002,** *19* (6), 357.
9. Madireddi, K.; Babcock, R.; Levine, B.; Kim, J.; Stenstrom, M., An unsteady-state model to predict concentration polarization in commercial spiral wound membranes. *J. Membr. Sci.* **1999,** *157* (1), 13-34.
10. Amokrane, M.; Sadaoui, D.; Koutsou, C.; Karabelas, A.; Dudeck, M., A study of flow field and concentration polarization evolution in membrane channels with two-dimensional spacers during water desalination. *J. Membr. Sci.* **2015,** *477*, 139-150.
11. Ahmad, A.; Lau, K.; Bakar, M. A.; Shukor, S. A., Integrated CFD simulation of concentration polarization in narrow membrane channel. *Comput. Chem. Eng.* **2005,** *29* (10), 2087-2095.
12. Santos, J.; Geraldes, V.; Velizarov, S.; Crespo, J., Investigation of flow patterns and mass transfer in membrane module channels filled with flow-aligned spacers using computational fluid dynamics (CFD). *J. Membr. Sci.* **2007,** *305* (1), 103-117.
13. Koutsou, C.; Yiantsios, S.; Karabelas, A., A numerical and experimental study of mass transfer in spacer-filled channels: effects of spacer geometrical characteristics and Schmidt number. *J. Membr. Sci.* **2009,** *326* (1), 234-251.
14. Shakaib, M.; Hasani, S.; Mahmood, M., CFD modeling for flow and mass transfer in spacer-obstructed membrane feed channels. *J. Membr. Sci.* **2009,** *326* (2), 270-284.
15. Subramani, A.; Kim, S.; Hoek, E. M., Pressure, flow, and concentration profiles in open and spacer-filled membrane channels. *J. Membr. Sci.* **2006,** *277* (1), 7-17.

16. Karode, S. K.; Kumar, A., Flow visualization through spacer filled channels by computational fluid dynamics I.: Pressure drop and shear rate calculations for flat sheet geometry. *J. Membr. Sci.* **2001,** *193* (1), 69-84.
17. Da Costa, A.; Fane, A.; Wiley, D., Spacer characterization and pressure drop modelling in spacer-filled channels for ultrafiltration. *J. Membr. Sci.* **1994,** *87* (1-2), 79-98.
18. Field, R.; Wu, D.; Howell, J.; Gupta, B., Critical flux concept for microfiltration fouling. *J. Membr. Sci.* **1995,** *100* (3), 259-272.
19. Bacchin, P.; Aimar, P.; Sanchez, V., Model for colloidal fouling of membranes. *AlChE J.* **1995,** *41* (2), 368-376.
20. Tang, C. Y.; Leckie, J. O., Membrane independent limiting flux for RO and NF membranes fouled by humic acid. *Environ. Sci. Technol.* **2007,** *41* (13), 4767-4773.
21. She, Q.; Tang, C. Y.; Wang, Y.-N.; Zhang, Z., The role of hydrodynamic conditions and solution chemistry on protein fouling during ultrafiltration. *Desalination* **2009,** *249* (3), 1079-1087.
22. Wang, Y.-N.; Tang, C. Y., Nanofiltration membrane fouling by oppositely charged macromolecules: Investigation on flux behavior, foulant mass deposition, and solute rejection. *Environmental Science & Technology* **2011,** *45* (20), 8941-8947.
23. Wang, Y.-N.; Tang, C. Y., Fouling of nanofiltration, reverse osmosis, and ultrafiltration membranes by protein mixtures: The role of inter-foulant-species interaction. *Environmental Science & Technology* **2011,** *45* (15), 6373-6379.
24. Thomas, D.; Judd, S.; Fawcett, N., Flocculation modelling: a review. *Water Res.* **1999,** *33* (7), 1579-1592.
25. Valioulis, I. A.; List, E. J., Collision efficiencies of diffusing spherical particles: hydrodynamic, van der Waals and electrostatic forces. *Adv. Colloid Interface Sci.* **1984,** *20* (1), 1-20.
26. Porter, M. C., Concentration Polarization with Membrane Ultrafiltration. *Industrial & Engineering Chemistry Product Research and Development* **1972,** *11* (3), 234-248.
27. Zydney, A. L.; Colton, C. K., A concentration polarization model for the filtrate flux in cross-flow microfiltration of particulate suspensions. *Chem. Eng. Commun.* **1986,** *47* (1-3), 1-21.
28. Kim, S.; Hoek, E. M. V., Modeling concentration polarization in reverse osmosis processes. *Desalination* **2005,** *186* (1-3), 111-128.
29. She, Q.; Hou, D.; Liu, J.; Tan, K. H.; Tang, C. Y., Effect of feed spacer induced membrane deformation on the performance of pressure retarded osmosis (PRO): Implications for PRO process operation. *J. Membr. Sci.* **2013,** *445*, 170-182.
30. Landau, L.; Lifshitz, E., Statistical physics, vol. 5. *Course of theoretical physics* **1980,** *30*.
31. Aimar, P.; Bacchin, P., Slow colloidal aggregation and membrane fouling. *Journal of Membrane Science* **2010,** *360* (1-2), 70-76.
32. Bacchin, P.; Aimar, P.; Field, R. W., Critical and sustainable fluxes: Theory, experiments and applications. *Journal of Membrane Science* **2006,** *281* (1-2), 42-69.
33. Kim, M. m.; Zydney, A. L., Theoretical analysis of particle trajectories and sieving in a two-dimensional cross-flow filtration system. *Journal of Membrane Science* **2006,** *281* (1-2), 666-675.
34. Zhang, G.; Zhang, J.; Wang, L.; Meng, Q.; Wang, J., Fouling mechanism of low-pressure hollow fiber membranes used in separating nanosized photocatalysts. *Journal of Membrane Science* **2012,** *389*, 532-543.
35. Weroński, P.; Elimelech, M., Novel numerical method for calculating initial flux of colloid particle adsorption through an energy barrier. *J. Colloid Interface Sci.* **2008,** *319* (2), 406-415.

509 36. Hoek, E. M.; Bhattacharjee, S.; Elimelech, M., Effect of membrane surface roughness
510 on colloid− membrane DLVO interactions. *Langmuir* **2003,** *19* (11), 4836-4847.
511 37. Jarusutthirak, C.; Amy, G., Role of soluble microbial products (SMP) in membrane
512 fouling and flux decline. *Environ. Sci. Technol.* **2006,** *40* (3), 969-974.
513 38. Bowen, W. R.; Hilal, N.; Lovitt, R. W.; Sharif, A. O.; Williams, P. M., Atomic force
514 microscope studies of membranes: force measurement and imaging in electrolyte solutions. *J.*
515 *Membr. Sci.* **1997,** *126* (1), 77-89.
516 39. Brant, J. A.; Childress, A. E., Membrane–colloid interactions: comparison of
517 extended DLVO predictions with AFM force measurements. *Environmental Engineering*
518 *Science* **2002,** *19* (6), 413-427.
519 40. Liu, G.; Yu, S.; Yang, H.; Hu, J.; Zhang, Y.; He, B.; Li, L.; Liu, Z., Molecular
520 mechanisms of ultrafiltration membrane fouling in polymer-flooding wastewater treatment:
521 role of ions in polymeric fouling. *Environ. Sci. Technol.* **2016,** *50* (3), 1393-1402.
522 41. Li, Q.; Elimelech, M., Organic fouling and chemical cleaning of nanofiltration
523 membranes: measurements and mechanisms. *Environ. Sci. Technol.* **2004,** *38* (17), 4683-
524 4693.
525 42. Tang, C. Y.; Kwon, Y.-N.; Leckie, J. O., Characterization of humic acid fouled
526 reverse osmosis and nanofiltration membranes by transmission electron microscopy and
527 streaming potential measurements. *Environ. Sci. Technol.* **2007,** *41* (3), 942-949.
528 43. Tang, C. Y.; Kwon, Y.-N.; Leckie, J. O., Fouling of reverse osmosis and
529 nanofiltration membranes by humic acid -- Effects of solution composition and
530 hydrodynamic conditions. *Journal of Membrane Science* **2007,** *290* (1-2), 86-94.
531 44. Tang, C. Y.; Kwon, Y.-N.; Leckie, J. O., Effect of membrane chemistry and coating
532 layer on physiochemical properties of thin film composite polyamide RO and NF membranes.
533 I. FTIR and XPS characterization of polyamide and coating layer chemistry. *Desalination*
534 **2009,** *242* (1-3), 149-167.
535 45. Tang, C. Y.; Kwon, Y.-N.; Leckie, J. O., Effect of membrane chemistry and coating
536 layer on physiochemical properties of thin film composite polyamide RO and NF membranes
537 II. Membrane physiochemical properties and their dependence on polyamide and coating
538 layers. *Desalination* **2009,** *242* (1-3), 168-182.
539 46. Ding, Y.; Tian, Y.; Li, Z.; Wang, H.; Chen, L., Microfiltration (MF) membrane
540 fouling potential evaluation of protein with different ion strengths and divalent cations based
541 on extended DLVO theory. *Desalination* **2013,** *331*, 62-68.
542 47. Ding, Y.; Tian, Y.; Li, Z.; Wang, H.; Chen, L., Interaction energy evaluation of the
543 role of solution chemistry and organic foulant composition on polysaccharide fouling of
544 microfiltration membrane bioreactors. *Chem. Eng. Sci.* **2013,** *104*, 1028-1035.
545 48. Li, Z.; Tian, Y.; Ding, Y.; Chen, L.; Wang, H., Fouling potential evaluation of soluble
546 microbial products (SMP) with different membrane surfaces in a hybrid membrane bioreactor
547 using worm reactor for sludge reduction. *Bioresour. Technol.* **2013,** *140*, 111-119.
548 49. Berg, O. G.; von Hippel, P. H., Diffusion-controlled macromolecular interactions.
549 *Annual review of biophysics and biophysical chemistry* **1985,** *14* (1), 131-158.
550 50. Hiemenz, P. C., *Principles of colloid and surface chemistry*. M. Dekker: 1977.
551 51. Lee, J. D.; Lee, S. H.; Jo, M. H.; Park, P. K.; Lee, C. H.; Kwak, J. W., Effect of
552 coagulation conditions on membrane filtration characteristics in coagulation - Microfiltration
553 process for water treatment. *Environmental Science and Technology* **2000,** *34* (17), 3780-
554 3788.

555